Supporting Information for

Free-standing Iridium and Rhodium-Based Hierarchically-Coiled Ultrathin Nanosheets for Highly Selective Reduction of Nitrobenzene to Azoxybenzene under Ambient Conditions

Zhi-Ping Zhang, Xin-Yu Wang,‡ Kun Yuan,‡ Wei Zhu, Tao Zhang, Yu-Hao Wang, Jun Ke, Xiao-Yu Zheng, Chun-Hua Yan, Ya-Wen Zhang*

Beijing National Laboratory for Molecular Sciences, State Key Laboratory of Rare Earth Materials Chemistry and Applications, PKU-HKU Joint Laboratory in Rare Earth Materials and Bioinorganic Chemistry, College of Chemistry and Molecular Engineering, Peking University, Beijing 100871, China.

1. Characterization of Hierarchically-Coiled Ir NSs.

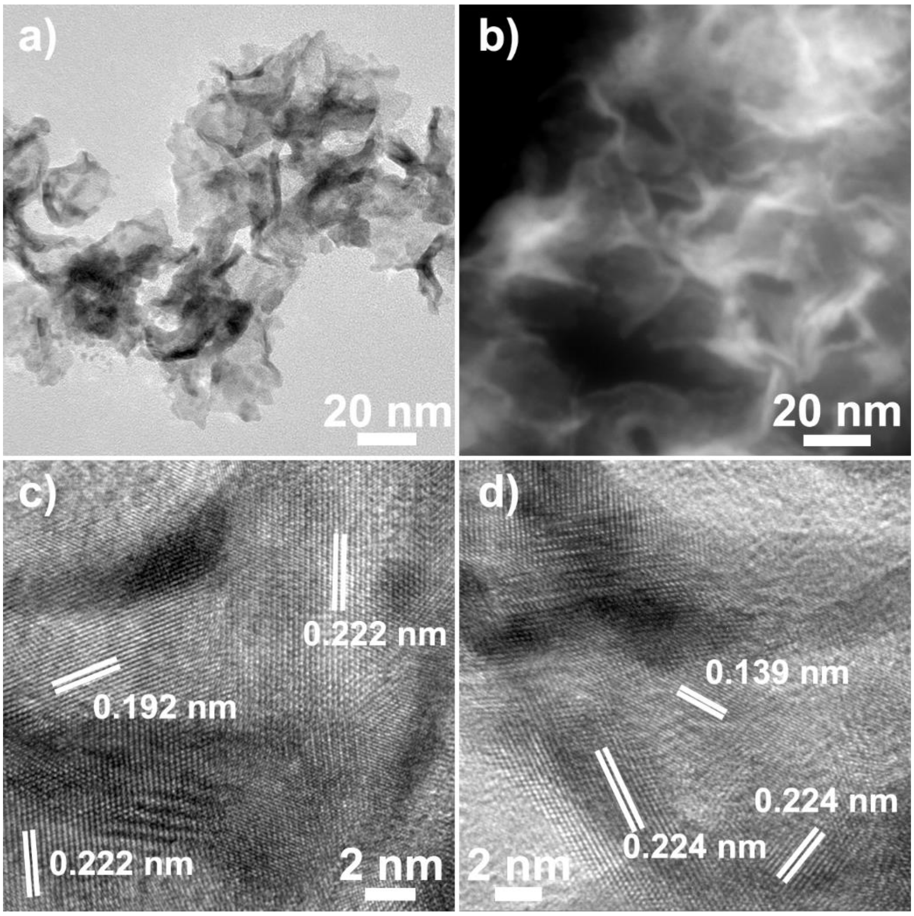

Fig. S1 (a) TEM image, (b) HAADF-STEM image and (c, d) HRTEM images of ultrathin Ir NSs.

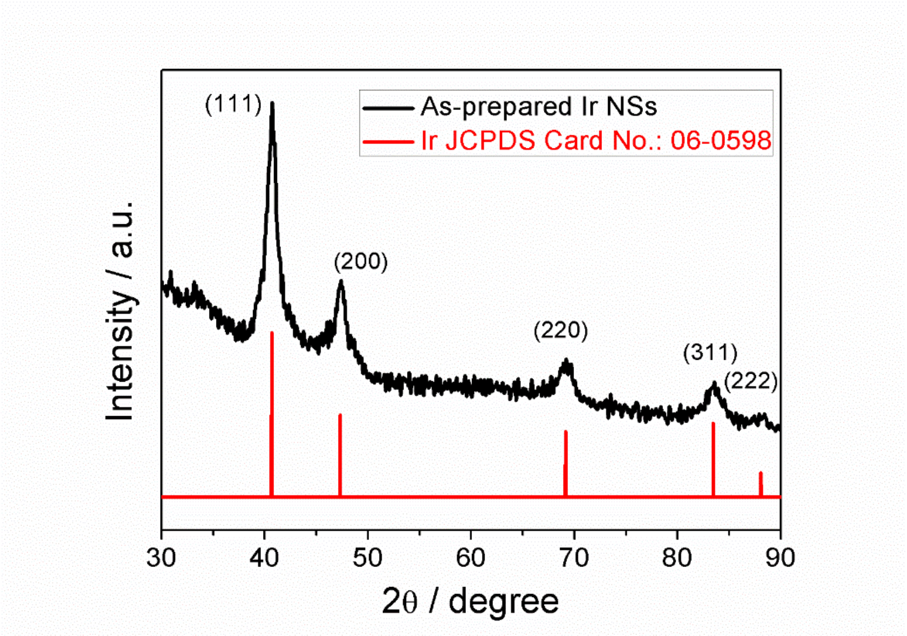

Fig. S2 XRD pattern of as-prepared Ir NSs, with the standard data for *fcc* Ir (JCPDS Card No.: 06-0598) as a reference.

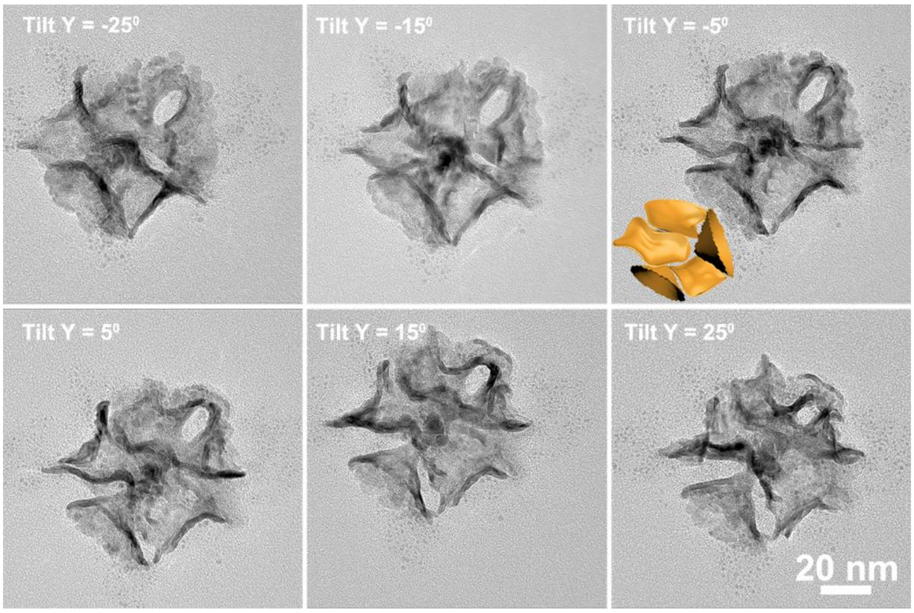

Fig. S3 TEM images of hierarchically-coiled ultrathin Ir NSs under various tilting angles along Y axis of the sample holder. Inset is the model of the hierarchically-coiled Ir NSs.

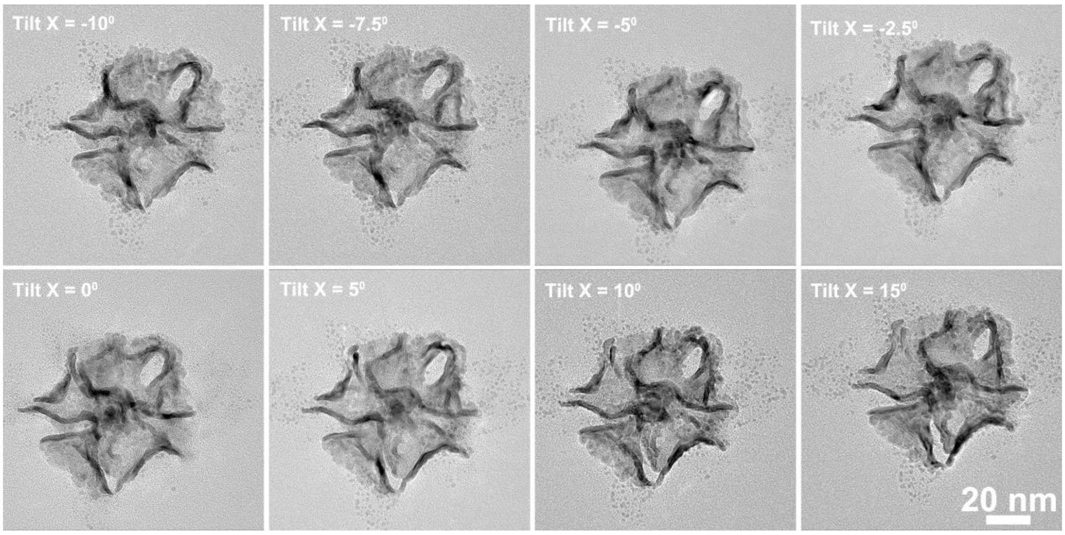

Fig. S4 TEM images of hierarchically-coiled ultrathin Ir NSs under various tilting angles along X axis of the sample holder.

.

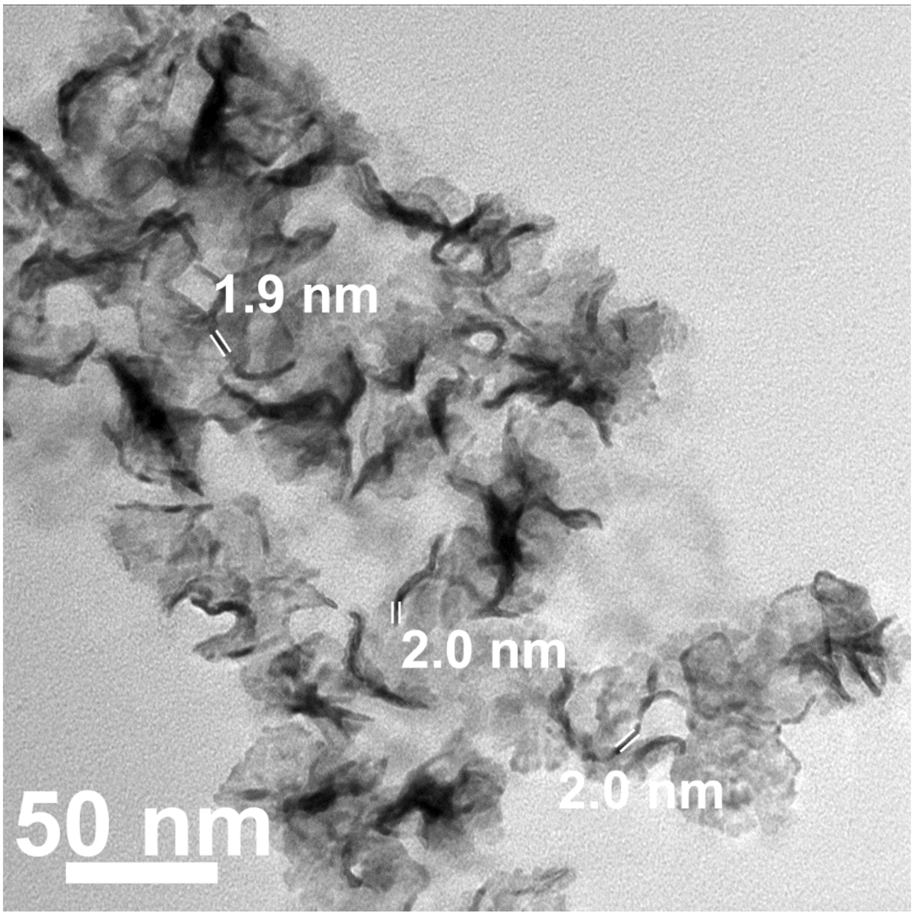

Fig. S5 TEM image of hierarchically-coiled ultrathin Ir NSs. Through the measurement of the edge width of ultrathin Ir NSs perpendicular to the TEM grid combined with the consideration of the curl of the edges, the thickness of the Ir NSs was estimated to be less than 2 nm.

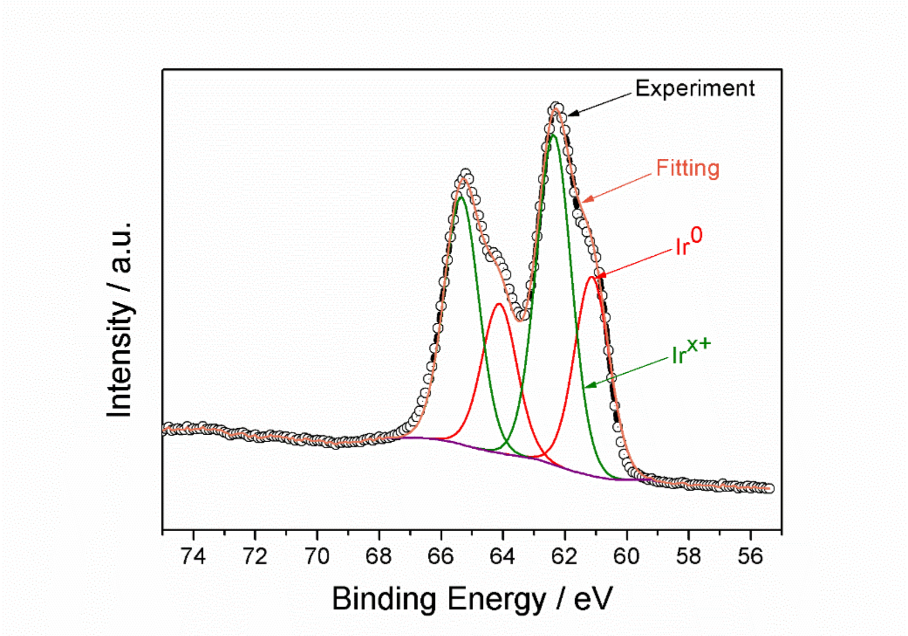

Fig. S6 Ir 4f XPS spectrum of Ir NSs. Through the calculation by dividing the sum of corrected area of the peak ascribed to Ir^0 4f (61.1 eV and 64.1 eV) by the total corrected area of Ir 4f, it was noted that 38% of Ir was in metallic state and 62% of Ir was in oxidized state (62.4 eV and 65.4 eV). It indicated a high proportion of Ir was oxidized on the surface of NSs due to the ultrathin size.

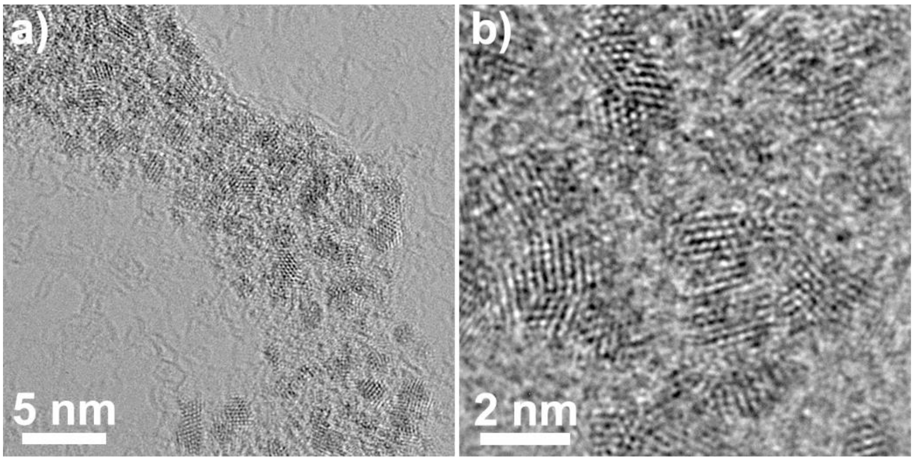

Fig. S7 TEM images of ultrathin Ir NSs formed at 1.5 h.

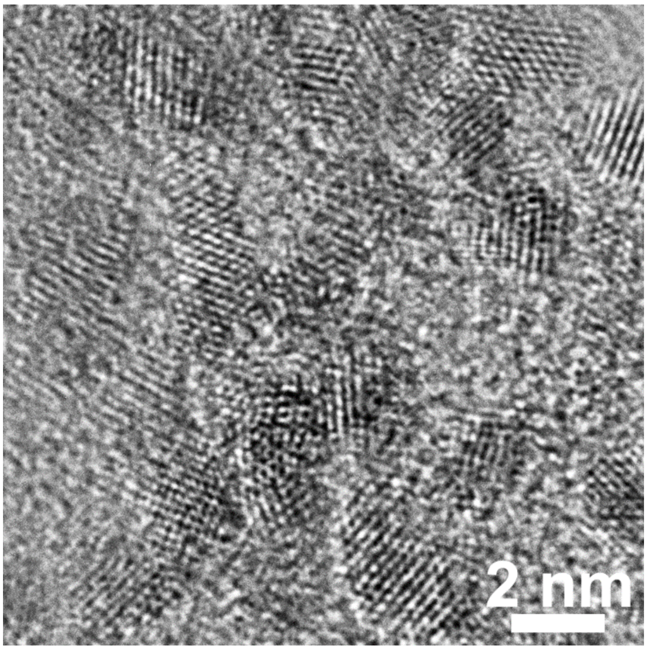

Fig. S8 TEM image of ultrathin Ir NSs formed at 3 h.

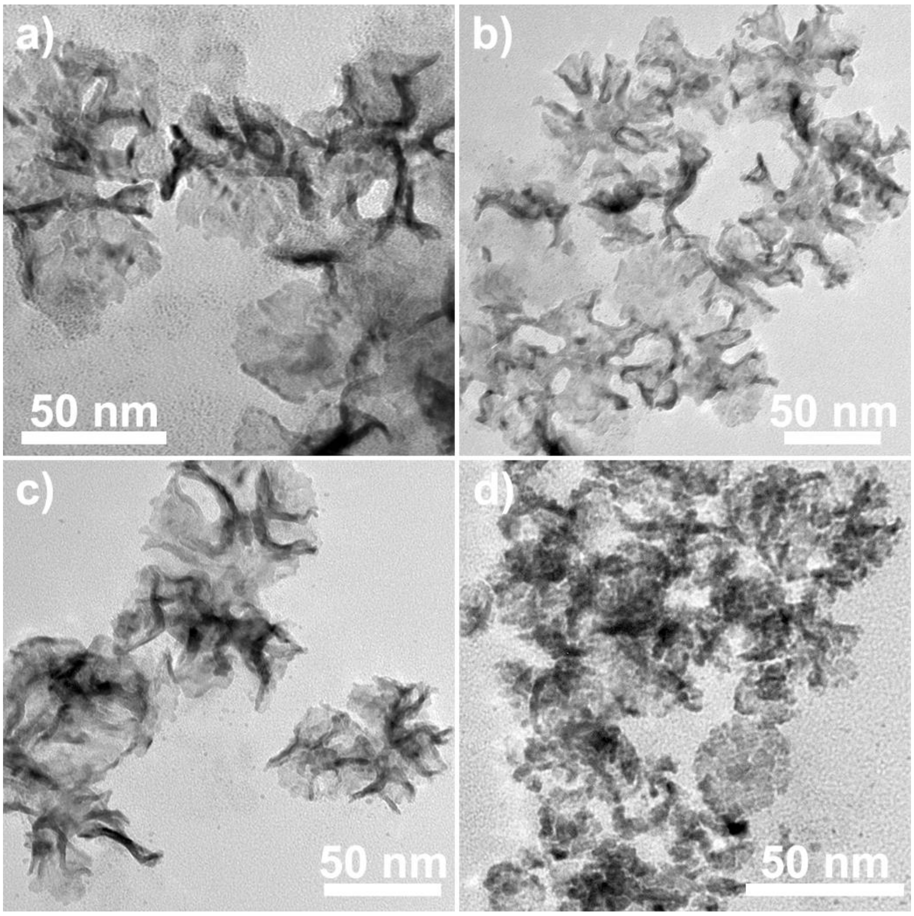

Fig. S9 TEM images of ultrathin Ir NSs synthesized with different amounts of *n*-butylamine: (a) none, (b) 50 μL, (c) 100 μL, (d) 200 μL.

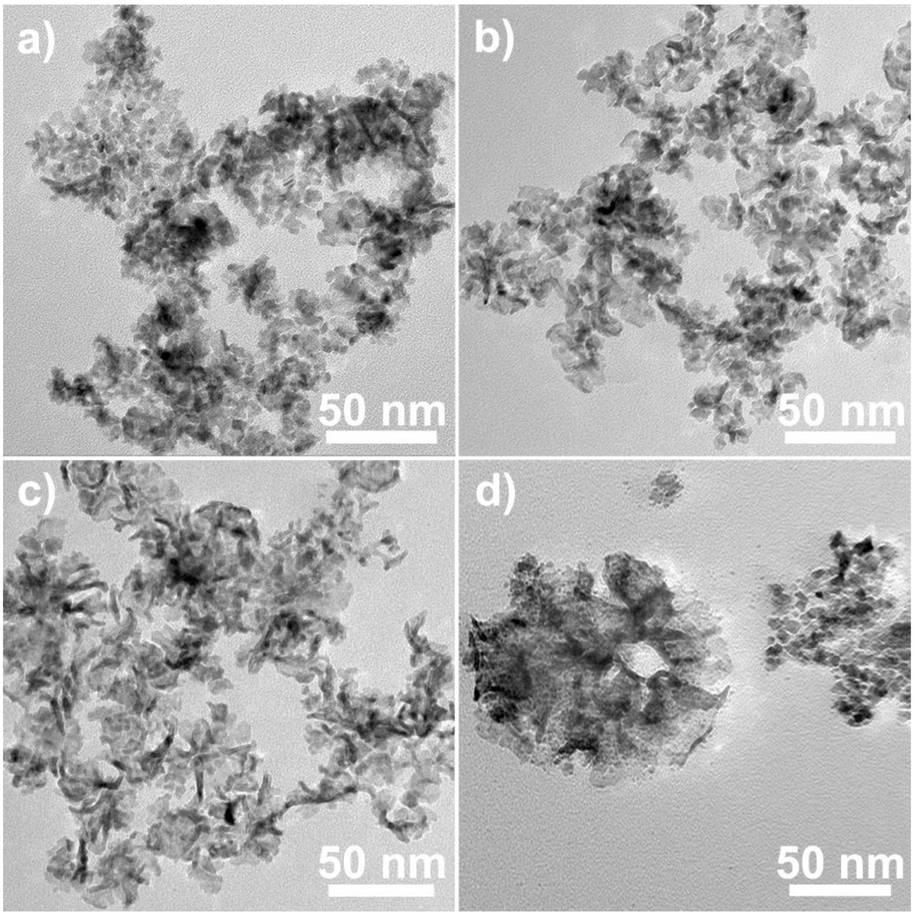

Fig. S10 TEM images of ultrathin Ir NSs synthesized with different amounts of $HCOONH_4$: (a) none, (b) 0.25 mmol, (c) 0.5 mmol, (d) 2 mmol.

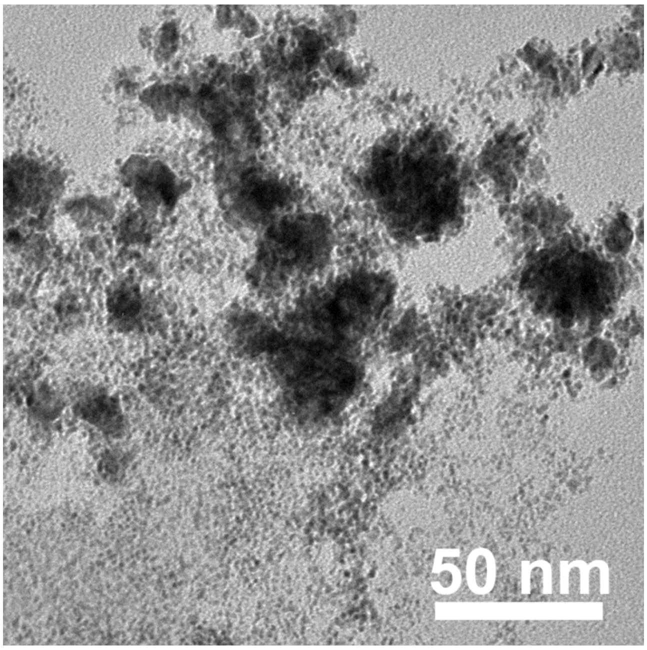

Fig. S11 TEM image of Ir NPs synthesized using HCOONa rather than $HCOONH_4$.

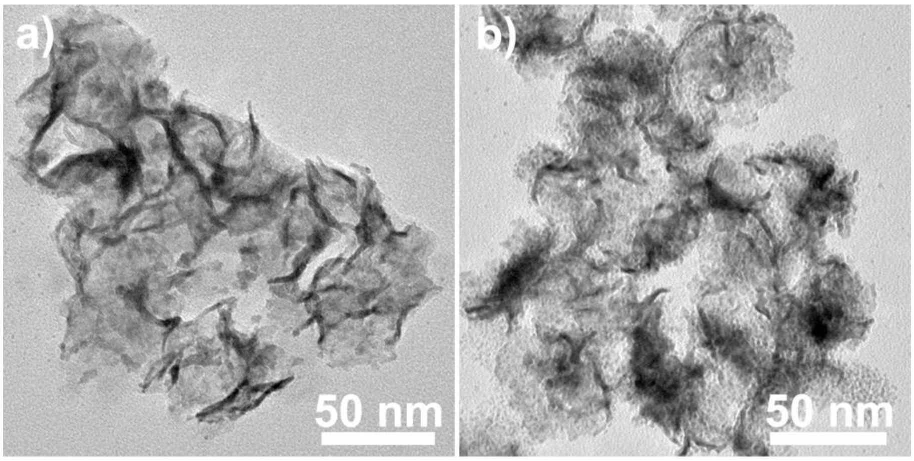

Fig. S12 TEM images of (a) ultrathin Ir NSs synthesized using gelatin rather than PVP and (b) Ir NPs synthesized without the surfactant.

.

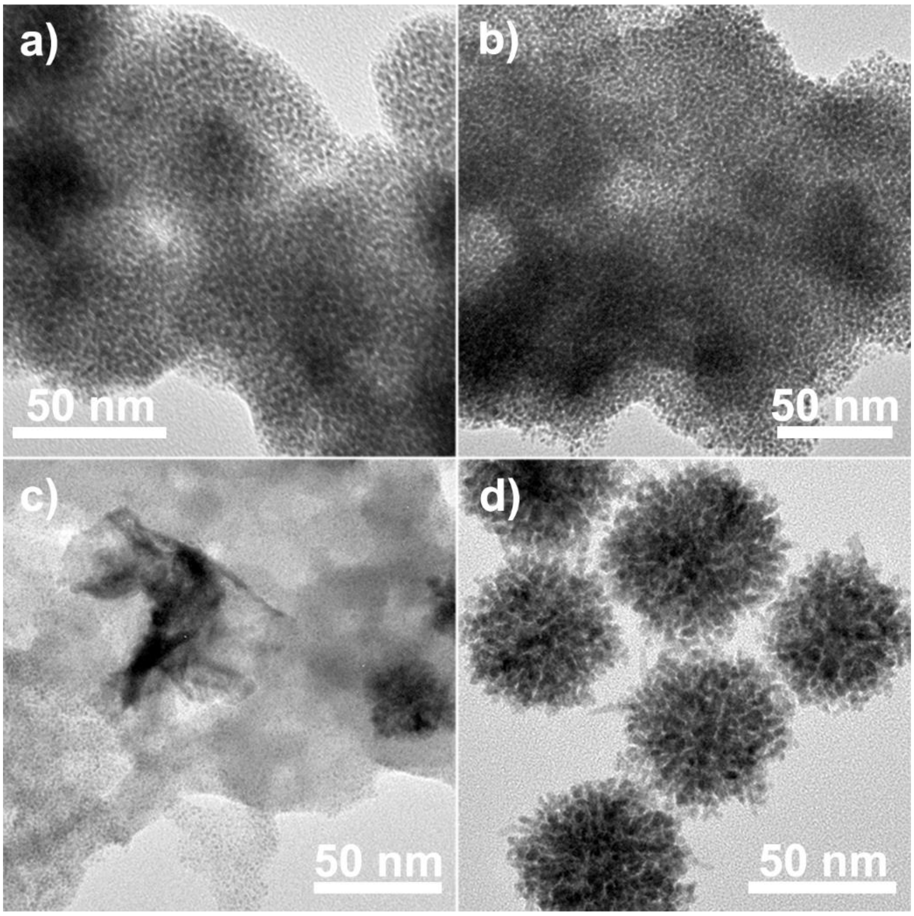

Fig. S13 TEM images of as-prepared Ir NPs formed in different solvents under 140 ℃: (a) ethylene glycol without n-butylamine, (b) diethylene glycol without n-butylamine, (c) 1-hexanol with n-butylamine and (d) using different precursor under 180 ℃: Ir(acac)$_3$.

2. Characterization of Hierarchically-Coiled Rh NSs, Ir-Rh NSs and Pt-Rh NSs.

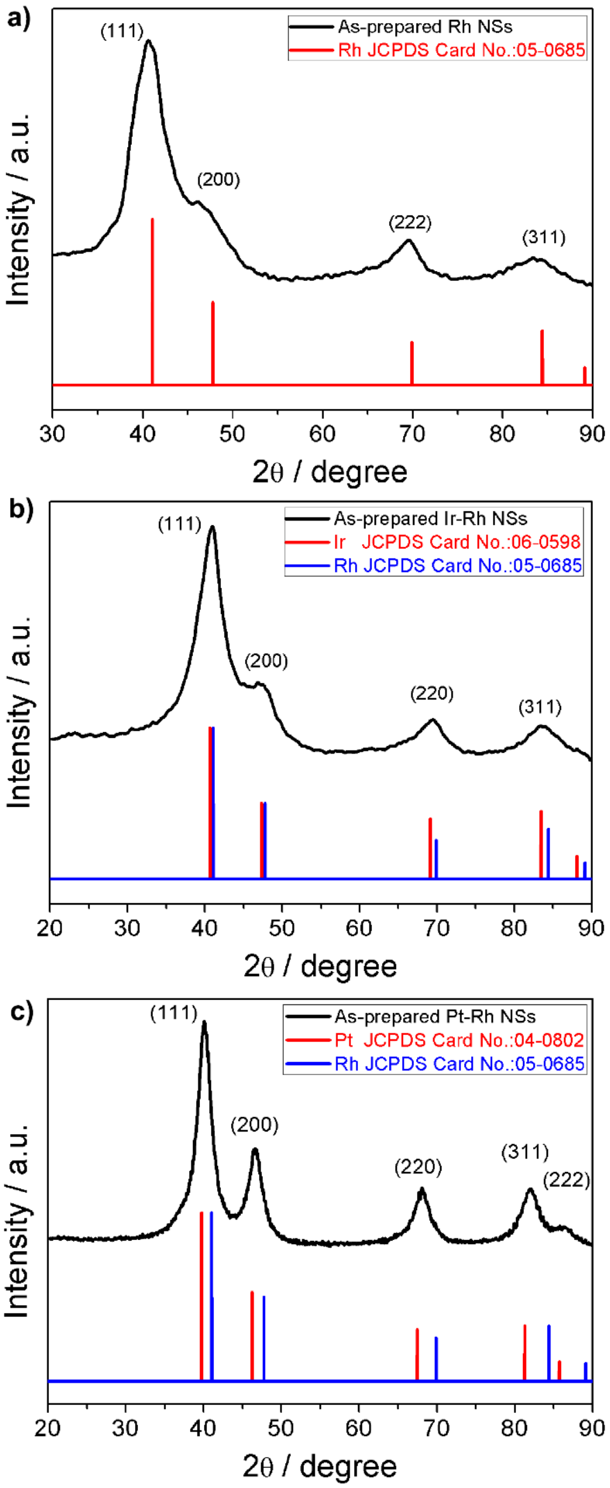

Fig. S14 XRD patterns of as-prepared (a) Rh NSs, (b) Ir-Rh NSs, (c) Pt-Rh NSs, with the standard data for *fcc* Rh (JCPDS Card No.: 05-0685), *fcc* Ir (JCPDS Card No.: 06-0598), *fcc* Pt (JCPDS Card No.: 04-0802) as references.

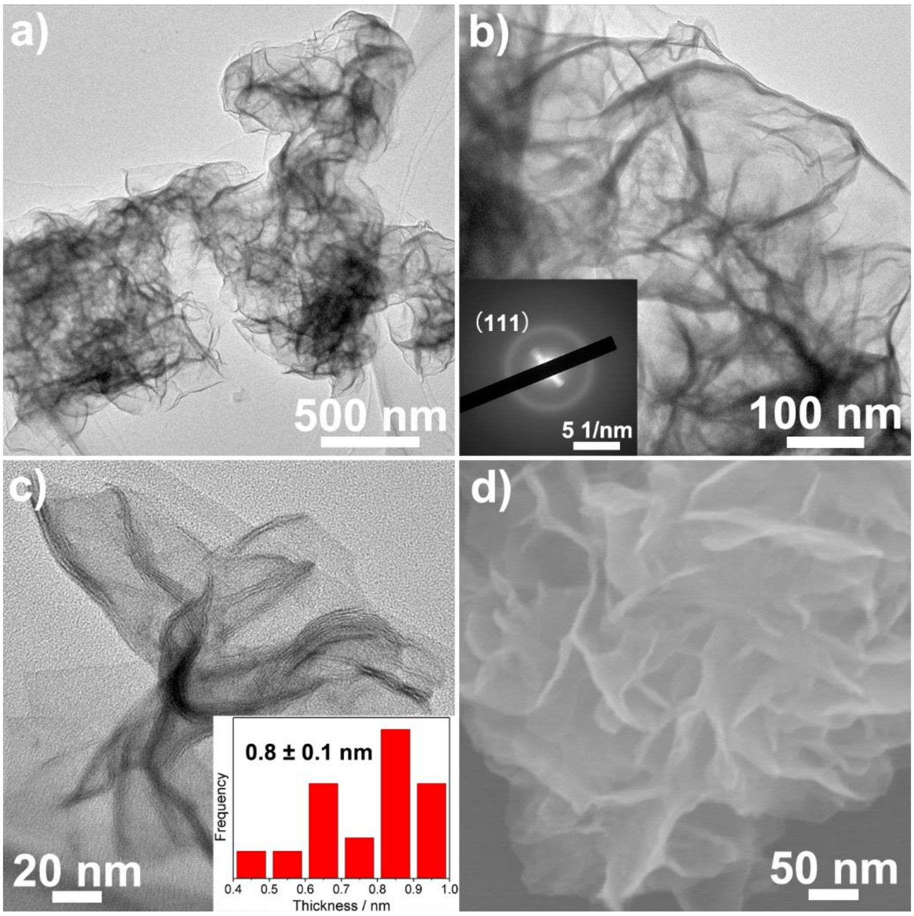

Fig. S15 (a, b, c) TEM images and (d) SEM image of ultrathin Rh NSs. Inset in panel b is the SAED pattern of Rh NSs, inset in panel c is the size distribution histogram of Rh NSs. Through the measurement of the edge width of ultrathin Rh NSs perpendicular to the TEM grid, the thickness of Rh NSs was 0.8±0.1 nm.

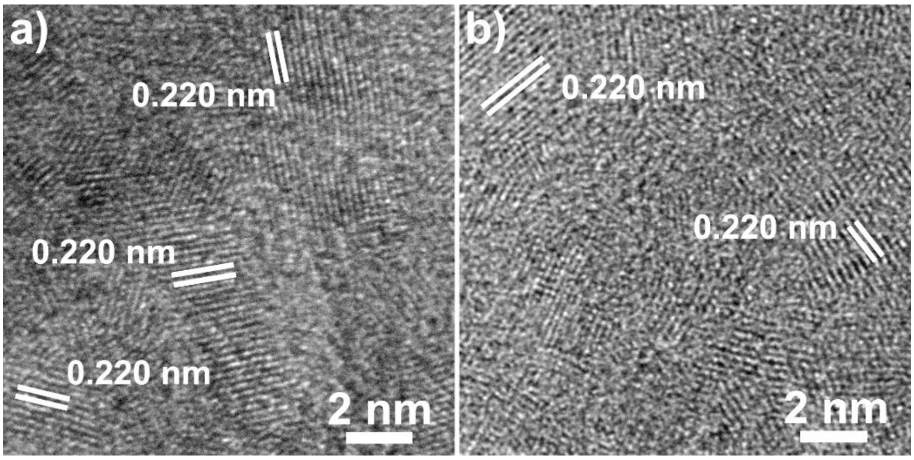

Fig. S16 (a, b) HRTEM images of ultrathin Rh NSs. The lattice fringes with inter-planar distances of about 0.220 nm correspond to the (111) plane of the fcc Rh. Only small nanodomains were short-range ordering, indicating Rh nanosheets have disordered structures and many defect sites (see Ref. S1).

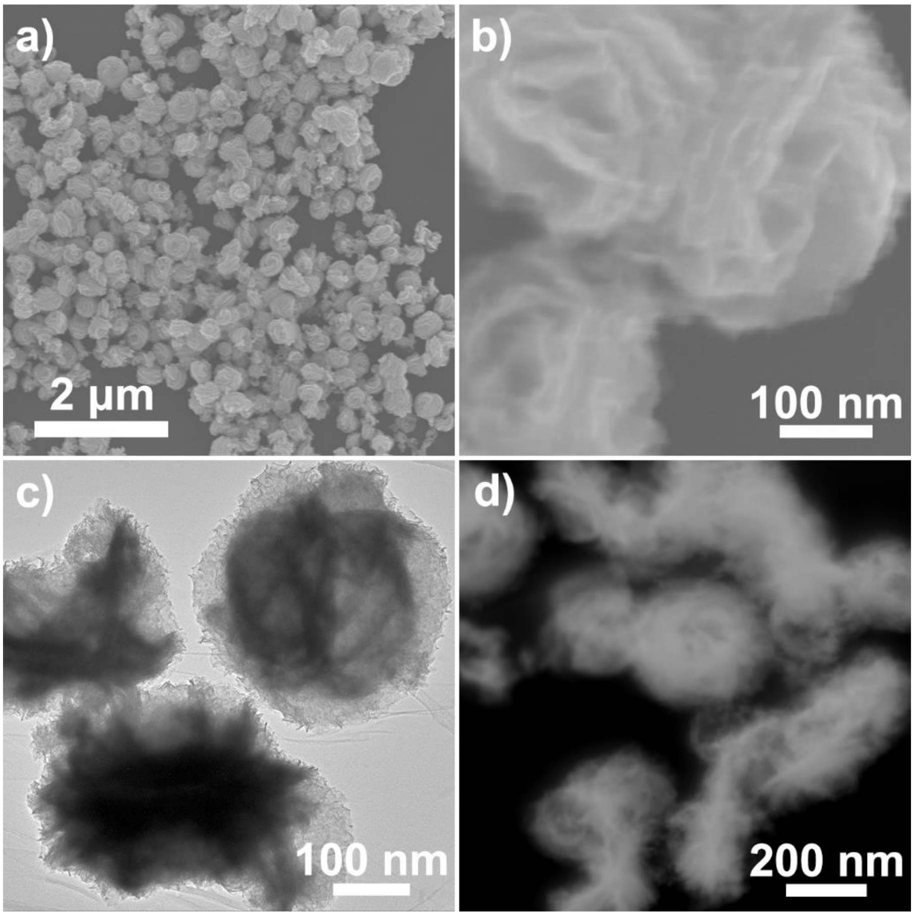

Fig. S17 (a, b) SEM images, (c) TEM image and (d) HAADF-STEM image of ultrathin Ir-Rh NSs.

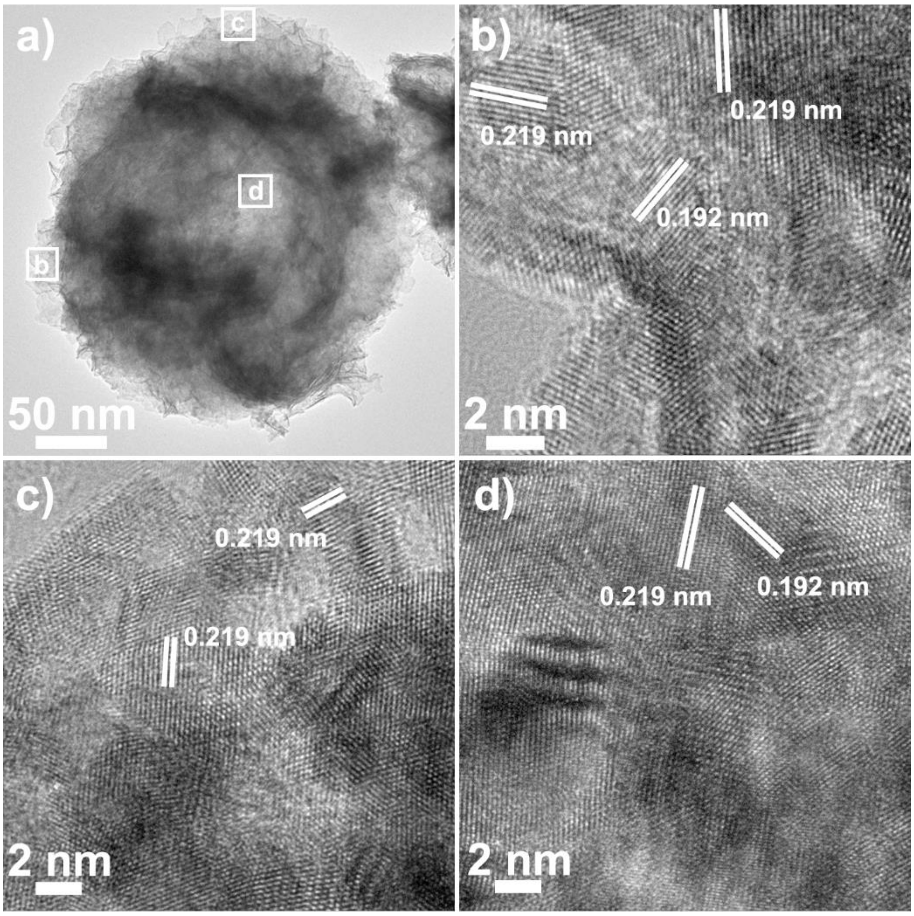

Fig. S18 (a) TEM image and (b, c, d) HRTEM images of ultrathin Ir-Rh NSs.

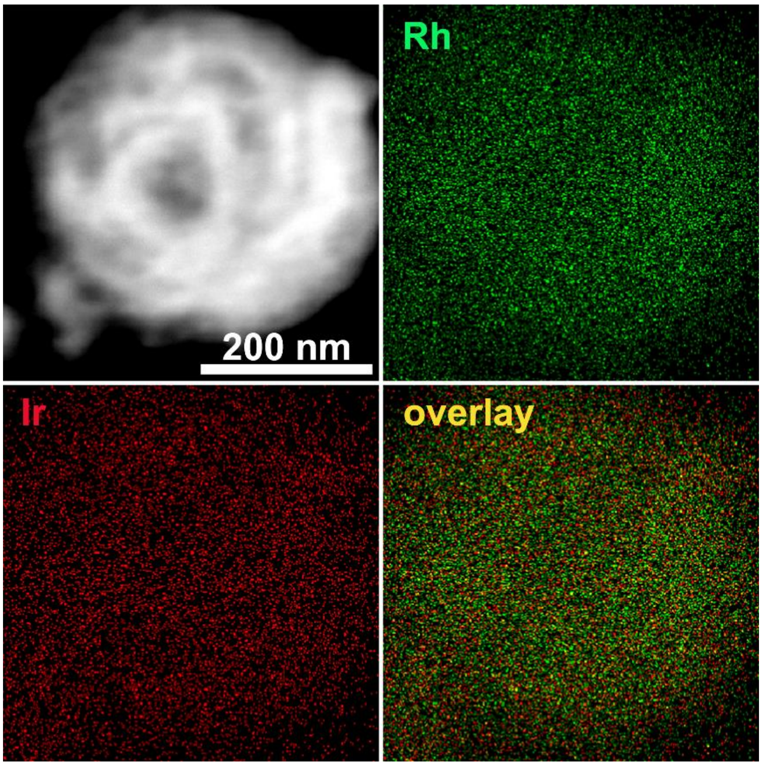

Fig. S19 EDS elemental mapping images of ultrathin Ir-Rh NSs.

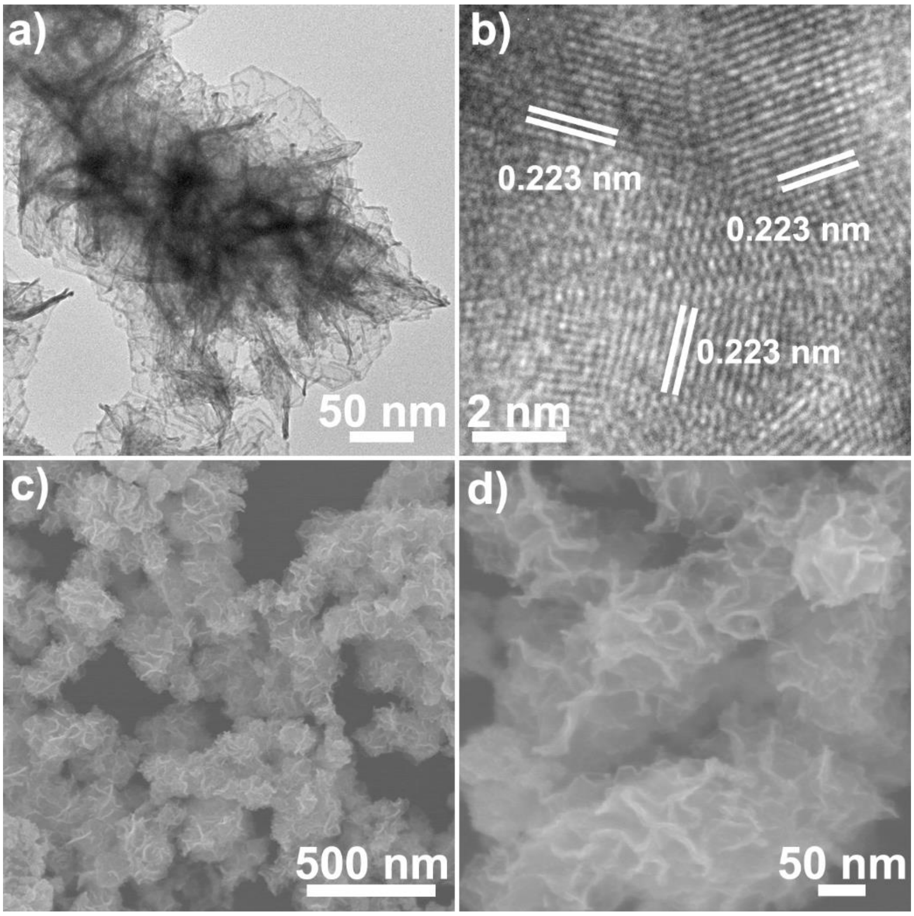

Fig. S20 (a) TEM image, (b) HRTEM image and (c, d) SEM images of ultrathin Pt-Rh NSs.

3. Selective reduction of nitrobenzene.

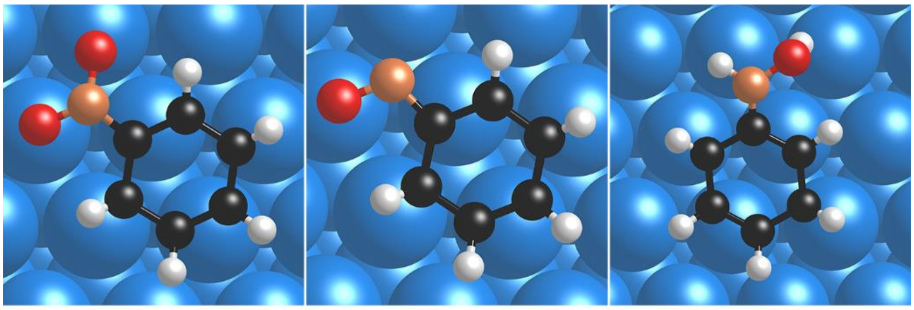

(a) $PhNO_2$ (b) PhNO (c) PhNHOH

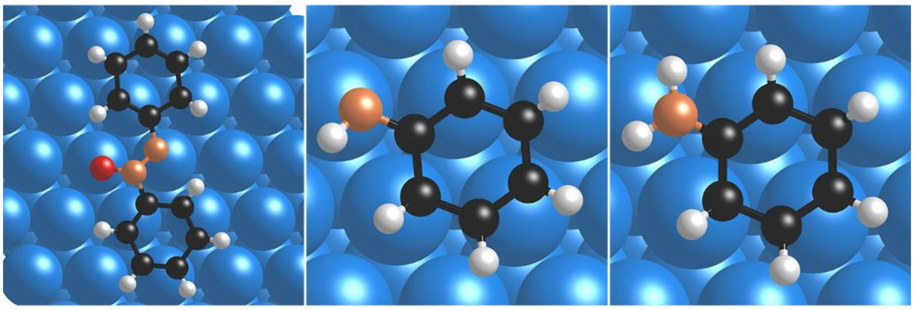

(d) PhN=NOPh (e) PhNH (f) $PhNH_2$

Fig. S21 Top views of different reaction species with most stable configurations on (111) facts of Ir NSs. Blue, black, white, orange, red atoms stand for Ir, C, H, N, O, respectively.

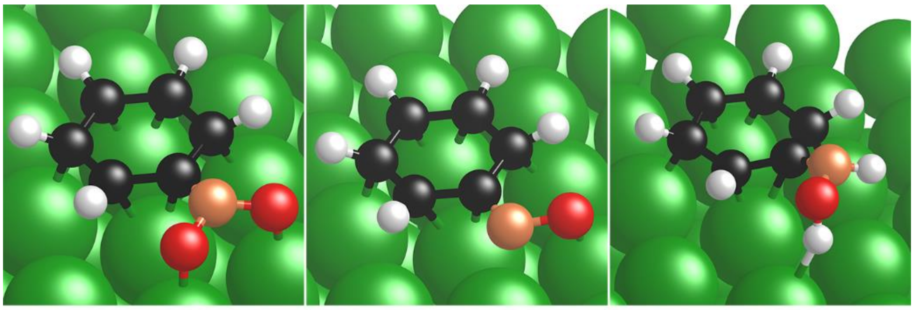

(a) $PhNO_2$ (b) PhNO (c) PhNHOH

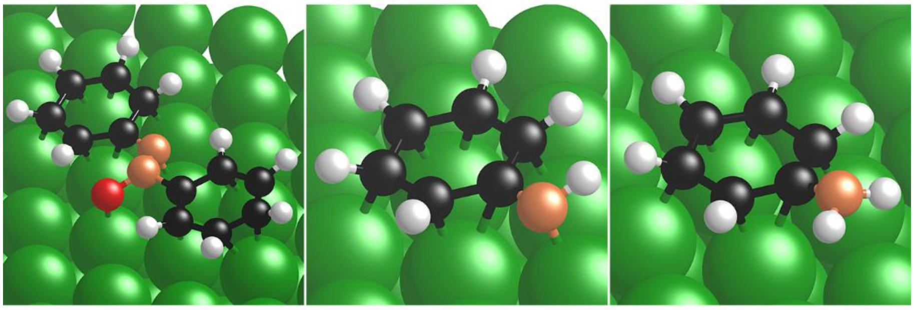

(d) PhN=NOPh (e) PhNH (f) $PhNH_2$

Fig. S22 Side views of different reaction species with most stable configurations on (111) facts of Rh NSs. Green, black, white, orange, red atoms stand for Ir, C, H, N, O, respectively.

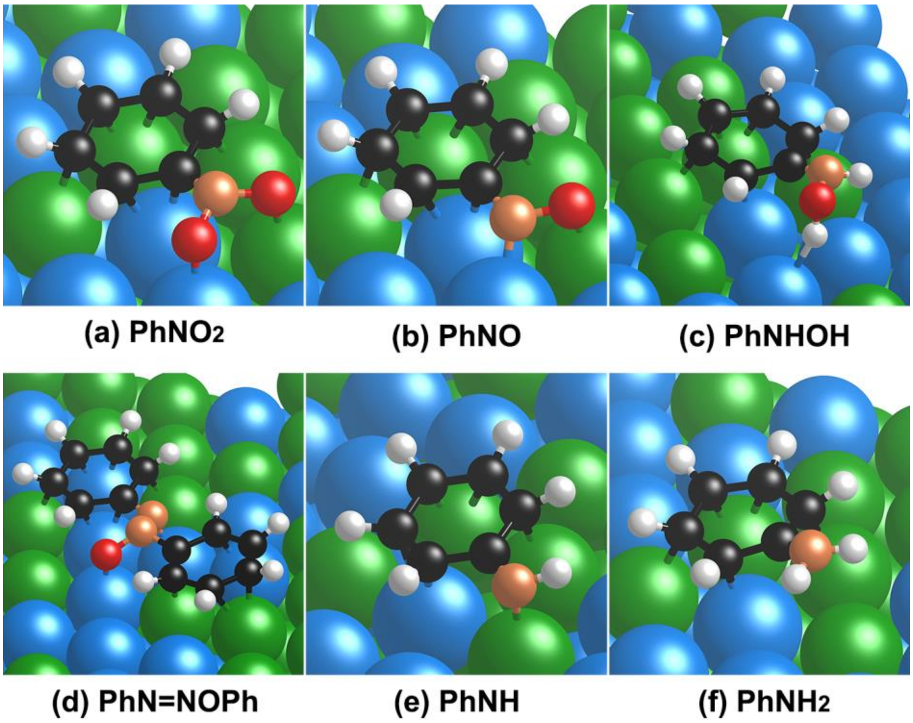

Fig. S23 Side views of different reaction species with most stable configurations on (111) facts of Ir-Rh NSs. Blue, Green, black, white, orange, red atoms stand for Ir, Rh, C, H, N, O, respectively.

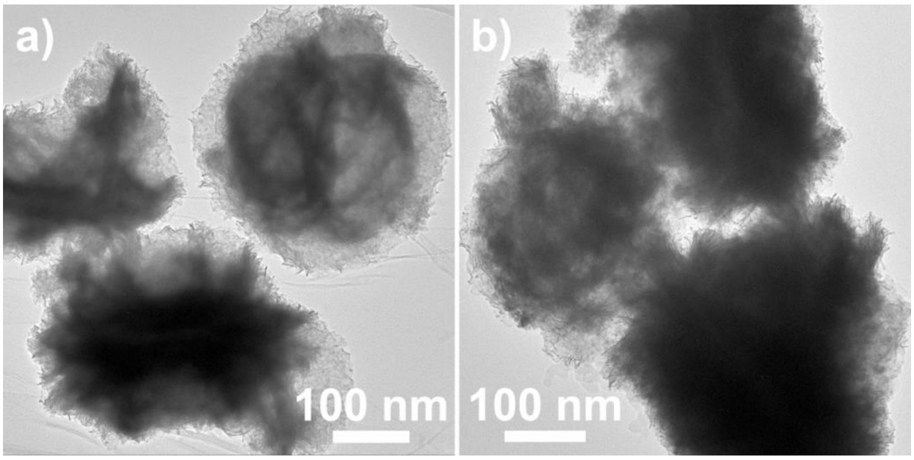

Fig. S24 TEM images of ultrathin Ir-Rh NSs (a) before catalytic reaction and (b) after the third reaction cycle.

Table S1 Selectivities of the different catalysts towards the formation of azoxybenzene via the reduction of nitrobenzene .

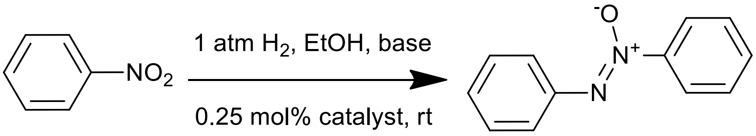

Entry	Catalyst	Time (h)	Conv. (%)	Select.(%) Azoxy
1	Ir NPs[a]	1.5	100	75.3
2	Rh NPs[b]	4	98.8	81.3
3	commercial 20% Ir/C	1.4	100	73.9
4	carbon black	1.4	0.4	0

[a] The synthesis of Ir NPs was the same as that of Ir NSs except without the addition of $HCOONH_4$ and *n*-butylamine. [b] The synthesis of Rh NPs was via the reduction of the solution of $RhCl_3$ and PVP by $NaBH_4$.

Table S2 Selectivities of the commercial Ir/C before and after the adsorption of PVP towards the formation of azoxybenzene via the reduction of nitrobenzene .

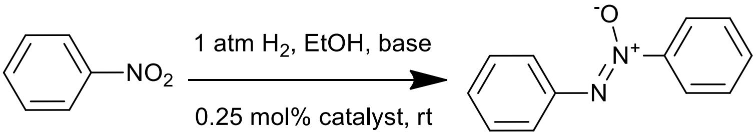

Entry	Catalyst	Time (h)	Conv. (%)	Select.(%) Azoxy
1	commercial 20% Ir/C	1.4	100	73.9
2	commercial 20% Ir/C after the adsorption of PVP[a]	1.4	75.8	76.6

[a] The sample was prepared via the following process: first, Ir/C was mixed with PVP in the ethanol solution by ultrasonic. After 12 h, the sample was centrifuged, followed by washing with ethanol and water for several times for the removal of free PVP.

Table S3 Total energies (eV) of different species with most stable configurations on Ir (111) facts.

Ph-NO_2	Ph-NO	Ph-NH	PhN=NOPh	Ph-NHOH
-899.222	-892.874	-891.847	-974.159	-901.231
Ph-NH_2	OH	H	H_2O	Ir
-896.134	-818.080	-810.423	-822.329	-806.641

Table S4 Total energies (eV) of different species with most stable configurations on Rh (111) facts

$Ph-NO_2$	Ph-NO	Ph-NH	PhN=NOPh	Ph-NHOH
-752.375	-746.388	-745.028	-827.810	-754.225
$Ph-NH_2$	OH	H	H_2O	Rh
-749.156	-669.934	-662.873	-673.900	-659.327

Table S5 Total energies (eV) of different species with most stable configurations on Ir-Rh (111) facts

$Ph-NO_2$	Ph-NO	Ph-NH	PhN=NOPh	Ph-NHOH
- 826.857	-820.713	-819.752	-902.163	-828.932
$Ph-NH_2$	OH	H	H_2O	Ir-Rh
- 823.852	-744.553	-737.982	-748.704	-734.168

Table S6 Adsorption energies (eV) of main final product (azoxybenzene) with most stable configurations on (111) facts of different NSs.

	Ir NSs	Rh NSs	Ir-Rh NSs
PhN=NOPh	-1.894	-2.859	-2.371

Table S7 Activities of the NSs catalysts towards the formation of azoxybenzene via the reduction of nitrobenzene using different bases.

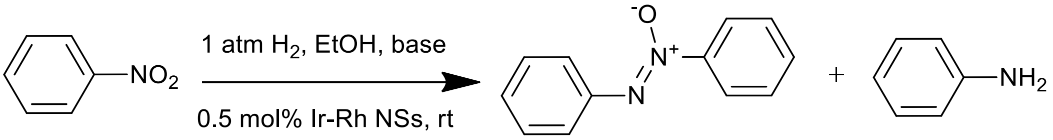

Entry	Base	Time (h)	Conv. (%)	Select.(%) Azoxy	Select. (%) Aniline	TOF (h^{-1})
1	none	3	27.2	13.8	27.2	18.1
2	200 μL butylamine	1.75	100	85.7	9.2	/
3	200 μL en	1.75	100	86.8	3.4	238

Reaction condition: 0.6 mmol of nitrobenzene as the reactant, 3×10^{-3} mmol of Ir-Rh NSs as the catalyst, and 2.8 mL of ethanol as the solvent, 1 atm hydrogen as the reductant, 25 ℃ as the reaction temperature.

Table S8 Cycle tests of the NSs catalysts towards the selective reduction of nitrobenzene.

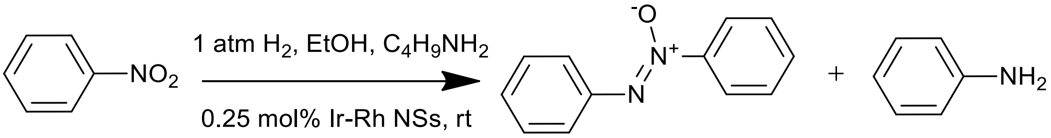

	Time (h)	Conv. (%)	Select.(%) Azoxy	Select.(%) Aniline
First	2.33	100	86.1	11.4
Second	2.33	100	84.1	15.3
Third	2.33	100	85.2	10.4

Reaction condition: 0.6 mmol of nitrobenzene, 200 μL of *n*-butylamine, 1.5×10^{-3} mmol of NSs (0.25 mol%), 2.8 mL of ethanol, 1 atm of H_2, 25 ℃. After each reaction cycle, the catalyst was separated by centrifugation, wash with ethanol, redispersed in ethanol for the next run.

4. References

Ref. S1 J. Xie, J. Zhang, S. Li, F. Grote, X. Zhang, H. Zhang, R. Wang, Y. Lei, B. Pan and Y. Xie, *J. Am. Chem. Soc.*, 2013, **135**, 17881-17888.